Soft Matter

Accepted Manuscript

ROYAL SOCIETY OF CHEMISTRY

www.rsc.org/softmatter

Journal Name

RSCPublishing

ARTICLE

Flattening of a Patterned Compliant Solid by Surface Stress

Cite this: DOI: 10.1039/x0xx00000x

Dadhichi Paretkar[a,b], Xuejuan Xu[c], Chung-Yuen Hui[c1], Anand Jagota[a*]

Received 00th January 2012,
Accepted 00th January 2012

DOI: 10.1039/x0xx00000x

www.rsc.org/

We measured the shape change of periodic ridge surface profiles in gelatin organogels resulting from deformation driven by their solid-vapor surface stress. Gelatin organogel was molded onto Poly-dimethylsiloxane (PDMS) masters having ridge heights of 1.7 and 2.7 μm and several periodicities. Gel replicas were found to have a shape deformed significantly compared to their PDMS master. Systematically larger deformations in gels were measured for lower elastic moduli. Measuring elastic modulus independently, we estimate a surface stress of 107±7 mN/m for the organogels in solvent composed of 70 wt% glycerol and 30 wt% water. Shape changes are in agreement with a small strain linear elastic theory. We also measured the deformation of deeper ridges (with height 13 μm), and analysed the resulting large surface strains using finite element analysis.

Introduction

Compliant amorphous solids such as elastomers and gels occupy an important place in current materials research. For sufficiently compliant materials, their surface stress can exert a significant influence on material behaviour by driving or resisting deformation. The surface stress of many elastomers and gels is isotropic and can be represented by a single number, σ[1–3]. How the shape of compliant solids is influenced by surface stress of the solid-fluid interface has been examined in several recent studies[4–9]. Often, surface stress plays a significant role when the characteristic material length scale, σ/E, exceeds some characteristic geometrical feature size, where E is the small strain Young's modulus[1,10]. For stiff solids such as metals and ceramics this characteristic material length scale is generally smaller than a nanometer and so the resulting deformations are very small and difficult to measure[10,11]. For compliant solids such as elastomers and gels, however, surface stress driven deformations can be macroscopic (tens to hundreds of μm) and can be readily measured. Mora *et al.* have observed an elastic Rayleigh-Plateau instability in a thin filament of solid hydrogel[6]. Similarly, when a thin elastomeric wire was immersed into a liquid a substantial elastic compression due to the solid capillary pressure was reported[8]. Deformation of thin elastomeric films due to liquid drops placed on their surface has been shown to be influenced strongly by surface stress[12,13]. We have previously shown that surface stress causes deformation of a ripple surface pattern in a hydrogel[9].

Here we present a study of the surface deformation of a compliant gelatin organogel patterned into a periodic ridge-channel shape. When the gel is released from the geometric constraint imposed by a PDMS mold consisting of periodic ridges (see Fig. 1a), the surface stress of the exposed gel/air interface causes the gel to deform. We measure the shapes of the master and the deformed gel, in particular, the reduction in the peak-to-valley distances (h) of the gel's surface features upon exposure to air. We systematically change the elastic modulus of the gels to change the amount of deformation caused by the surface stress. The elastic modulus of the gels is determined independently using beam bending and punch tests (see SI). The surface stress of the gels is determined by comparing measured deformation to the prediction of models for surface-stress-driven elastic deformation. Our results suggest that shape change for nearly flat surfaces in the case of simple geometries such as periodic ridges can be used for determination of surface stress of compliant solids.

Experimental

Fabrication of periodic ridge samples

Polydimethylsiloxane (PDMS) surfaces structured with a periodic ridge geometry were used to replica-mold gelatin gels (Figure 1). Three sets of ridge geometries, one with height (h) of 13 µm and two others with lower heights of 1.7 and 2.7 µm were used in this work. For the lower height ridge geometries the width (w) of the ridge was kept the same as the spacing (s) between the ridges, whereas for the high ridge geometry three different periods λ ($\lambda = w + s$) were fabricated. Height, h, is taken as the initial peak-to-valley distance for the gel sample i.e. prior to its demolding (assuming that the gel fills the PDMS master without any air cavities[9]).

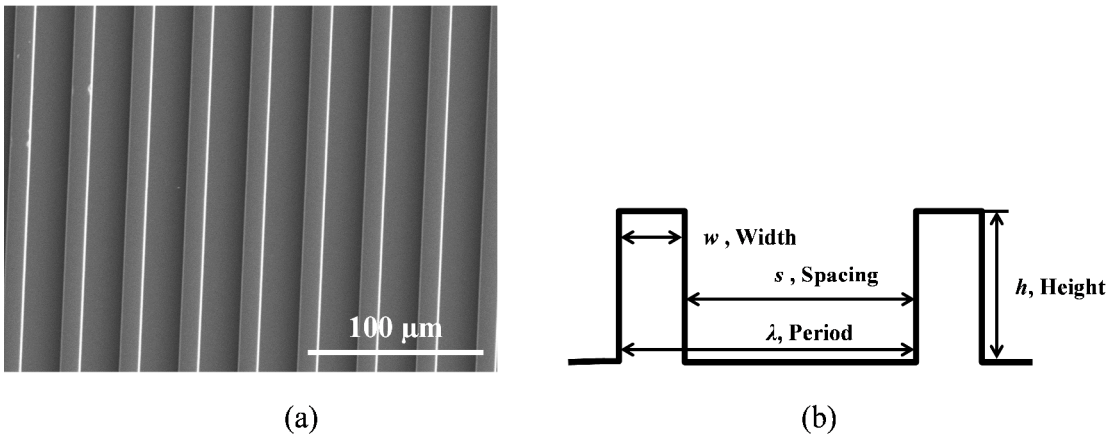

Figure 1: (a) SEM image of a typical PDMS master periodic ridge geometry. (b) Schematic of the periodic ridge geometry.

Table 1 lists the details of the periodic ridge geometry. The fabrication details for surface structuring of PDMS with ripple geometries are described in detail elsewhere [14].

Table 1. *Dimensions (with standard deviations) of periodic ridge geometry. For the case of lower height ridges (h ~1.7 and 2.7 µm) the width was not measured separately but was estimated in the model as half of the mean period.*

Ridge/channel h [µm]	Period λ_1 [µm]	Period λ_2 [µm]	Period λ_3 [µm]	Ridge width w [µm]
1.68±0.03	-	39.68±0.52	49.39±0.39	$\lambda/2$
2.66±0.05	24.82±0.49	39.77±0.37	49.54±0.29	$\lambda/2$
13.16±0.15	34.55±1.12	49.42±0.64	64.90±0.87	10.91±0.21

High temperatures and continuous stirring were employed to obtain homogenous pre-gel mixtures following Baumberger *et al.* [15]. Organogels were prepared by dissolving 7.5, 10, 12.5 and 15 wt% gelatin powder (type A from porcine skin, Sigma Aldrich) in mixtures of 70 wt % glycerol - 30 wt% deionized water, followed by continuous stirring at 85 °C for 4 hours. This was followed by an additional hour of heating without stirring to allow the air bubbles to escape the pre-gel mixture. The pre-gel mixture was poured into a petri dish containing the structured PDMS mold placed with its structured side facing up. The liquid gel filled the PDMS mold and rose to a thickness of about 2 mm above the PDMS surface. The liquid wets the PDMS surface completely and upon cross-linking takes the shape of the PDMS surface (see SI and [9]). The pre-gel mixture was allowed to cool and cross-link at room temperature for about 10-15 min after pouring. Subsequently, the mold was placed in a refrigerator at 4 °C for 16.5 h to complete the gelation process. The gel was then removed and allowed to equilibrate to room temperature for 1 h prior to demolding and gel characterization.

The gel and PDMS surface profiles were measured using an optical profilometer (Zemetrics ZeGage, Zygo Corp. CT USA).

Measurement of Elastic Modulus

Elastic moduli of the gel samples were measured independently by beam-bending and a contact compliance method. In the contact compliance method, a polished steel cylindrical flat probe is indented on the flat surface of a block of gelatin gel (30x30 mm and 4-5 mm thick) at a constant speed of 1 µm/s to a pre-defined indentation depth (~50-150 µm) and retracted at the same speed to the starting position. The indenter radius (~ 1mm) is small in comparison to the lateral dimensions of the gel block. The contact was monitored using a microscope. The force and the indentation depth during indentation/retraction were recorded using a load cell (Honeywell Ltd.) and a capacitive displacement sensor, respectively. The compliance of the sample was determined from the slope of the force versus indentation depth curve and the Young's modulus was computed following Rong *et al.* [16] (details in supplementary information). Beam bending tests were additionally performed as an independent modulus measurement (see SI for detailed description). The Young's moduli of the gels range from 14-50 kPa. We also studied the effect of loading rate by conducting indentations at different rates (0.01-10 µm/s) and found no significant difference in the measured Young's modulus.

Results

Experimental results

a) Periodic ridge geometry h ~ 2.7 and 1.7 µm

Figure 2 (a) shows a 3D surface profile of a PDMS mold with a periodic ridge-channel geometry against which a gel with Young's modulus E = 32.5 kPa was molded. The measured surface profile of the demolded gel sample is shown alongside.

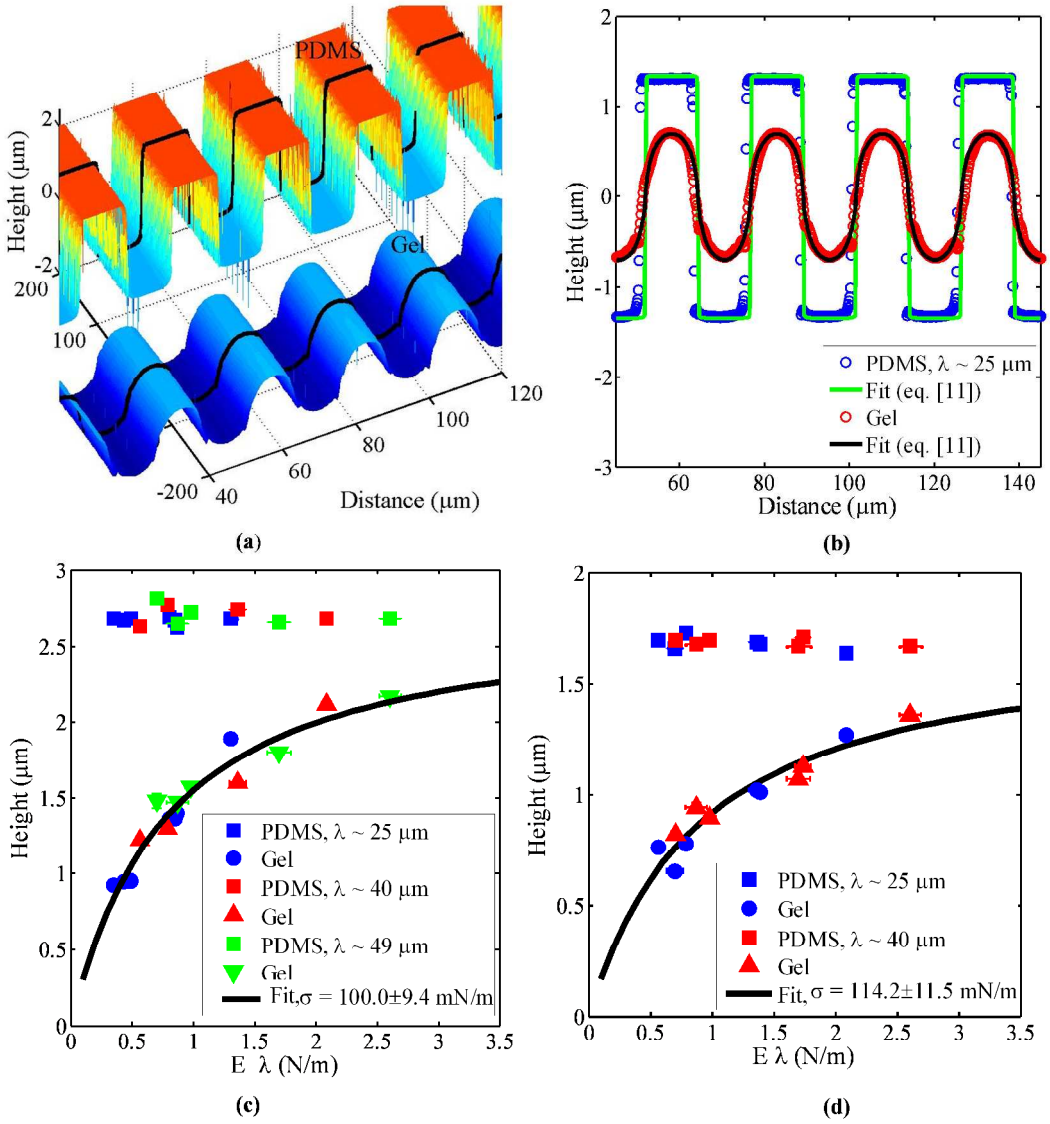

Figure 2: (a) Measured 3D surface profile of periodic ridge geometry showing PDMS master and its gel replica for E = 32.5 kPa, $\lambda \sim$ 25 μm and initial height $h \sim 2.7$ μm. The black lines over the surface profiles represent the position of the line scan in (b). (b) Line scans of the PDMS and gel surface profiles (circle symbols) and the theoretically predicted PDMS and gel profiles (continuous lines) using eq. [11] and a single fitting parameter of σ = 100.0 mN/m for the deformed shape. (PDMS and gel profiles have been shifted with respect to the y-axis such that their mean lies around zero) (c) Final gel height (h_d) (symbols circles, triangles and inverted triangles represent, respectively, spacings $\lambda \sim$ 25, 40 and 49 μm) compared to (initial) PDMS (square symbols) with ridge height $h \sim$ 2.7 μm (d) $h \sim 1.7$ μm as a function of several elastic moduli (E) and periodic separations (λ). Least Square fits using eq. [11] (solid black lines in (c) and (d)) estimate the surface stress to be 100.0±9.4 mN/m and 114.2±11.5 mN/m (95% confidence) for $h \sim 2.7$ and 1.7 μm respectively.

We observe that the gel profile is significantly rounded compared to the sharply edged periodic ridges of the PDMS master into which it was molded. The deformed height (h_d) and the rounding of the edges create a sinuous profile, which can be seen from the line scans (Figure 2(b)) of the surfaces of the gel sample and the PDMS master. Using small strain theory the entire surface profiles (eq. [11] below, continuous lines, Figure 2 (b)) for the PDMS (which is the same as the undeformed gel for σ = 0 mN/m) and the deformed gel (σ = 100 mN/m) were evaluated and plotted alongside experimental data. For the shallow profiles, the theory based on small strain elasticity fits the data well.

Figure 2 (c) and (d) shows the measured ridge height of PDMS master (h) (square symbols) and its gel replica (h_d) after demolding. The maximum height (peak to valley) of the deformed sample (h_d) are plotted against the product of periodic spacing (λ) and elastic modulus (E) of the gels (symbols circles, triangles and inverted triangles represent, respectively, spacings $\lambda \sim$ 25, 40 and 49 μm). A systematic reduction in the gel height h with reduction in the gel modulus was observed. Least square fits to the experimental data using the small strain theory (eq. [11]) are plotted for the two initial heights, $h \sim 2.7$ μm (figure 2 (c)) and $h \sim 1.7$ μm (figure 2 (d)). The fits are generated using a single fitting parameter, the mean surface

stress, of σ= 100.0 and σ=114.2 mN/m for h ~ 2.7 and 1.7 µm, respectively. We further determined the accuracy of the fitted surface stress [17] and found, with a confidence of 95%, that σ= 100.0±9.4 mN.

b) Analysis of deformation driven by surface stress

To analyse the shape change we assume that deformation is driven by the surface stress. Further, we have assumed that the boundaries are traction free and the material is elastic. There is little change observed experimentally in the dimension parallel to the ridges, hence we use a plane strain condition.

When the ridges are shallow, the deformation is small, and a closed form approximate solution can be obtained based on a scheme used by Hertz to compute the deformation of elastic spheres in contact [18]. Specifically, instead of applying the Laplace pressure on the deformed surface, which is not flat, we determine the deformation caused by the Laplace pressure by imposing it on a flat elastic half space. This procedure is valid provided that the curvature of the deformed surface is small. Since periodic ridge surface profiles can be represented by a Fourier series, the undeformed surface profile $y_0$is

$$y_0 = c_0 + \sum_{n=1}^{\infty} a_n^0 cos\left(\frac{2\pi nx}{\lambda}\right) \quad [1]$$

where (c_0, a_n^0) are Fourier coefficients. The deformed surface profile, after peeling the gel off the PDMS master is given by

$$y = c + \sum_{n=1}^{\infty} a_n cos\left(\frac{2\pi nx}{\lambda}\right) \quad [2]$$

The Laplace pressure p that causes the surface flattening is equal to the product of surface stress and curvature which we assume to be small. Using [2],

$$p = \sigma y'' = -\sum_{n=1}^{\infty} a_n \sigma \left(\frac{4\pi^2 n^2}{\lambda^2}\right) cos\left(\frac{2\pi nx}{\lambda}\right) \quad [3]$$

The Laplace pressure is calculated based on the unknown final shape (eq.[2]), not the initial shape. For this reason, although the kinematics and elasticity is linear, the final result relating shape change to the surface stress that drives it is nonlinear. As mentioned earlier, the vertical displacement u caused by the Laplace pressure (eq. [3]) was computed based on the elastic solution of a periodic normal traction acting on the surface of a flat elastic half space [19]. Using superposition, u is found to be:

$$u = -\sum_{n=1}^{\infty} 4\pi \left(\frac{a_n n}{\lambda}\right)\left(\frac{\sigma}{E^*}\right) cos\left(\frac{2\pi nx}{\lambda}\right) \quad [4]$$

The final and the initial shapes of the surface are related to each other by

$$y = y_0 + u \quad [5]$$

The relation between the Fourier coefficients of y_0 and y can be found using [1], [2], [4] and [5], which results in

$$a_n = \frac{a_n^0}{1+4\pi\left(\frac{\sigma n}{\lambda E^*}\right)}; c = c^0 \quad [6]$$

Equation [6] shows that the higher Fourier modes (larger n) are attenuated by surface stress to a greater extent than are modes with smaller n. The Fourier coefficients of the undeformed profiles are

$$a_n^0 = \frac{2h}{n\pi} sin\left(\frac{n\pi w}{\lambda}\right); c_0 = \frac{hw}{\lambda} \quad [7]$$

The shape of the deformed profile can be found using [6], [7] and [2], resulting in

$$y = \frac{hw}{\lambda} + \frac{2h}{\pi}\sum_{n=1}^{\infty} \frac{sin\left(\frac{n\pi w}{\lambda}\right)}{n\left[1+4\pi\left(\frac{\sigma n}{\lambda E^*}\right)\right]} cos\left(\frac{2\pi nx}{\lambda}\right) \quad [8]$$

The peak to valley height of the deformed profile is

$$h_d = \sum_{n=1}^{\infty} a_n - \sum_{n=1}^{\infty}(-1)^n a_n$$

$$= \frac{4h}{\pi}\sum_{n=1}^{\infty} \frac{\sin\left[\frac{(2n-1)\pi w}{\lambda}\right]}{(2n-1)\left(1+4\pi\frac{\sigma(2n-1)}{\lambda E^*}\right)} \quad [9]$$

Figure 3 shows the shape change of a gel replica with increasing surface stress predicted using eq. [8] (500 terms were included in the calculation). As seen already in Figure 2b, compared to the initial sharp edges present in the periodic ridge profile, the deformed shape of the gel has significantly rounded edges.
Equations [8] and [9] were used to fit the data shown in Figure 2.

c) Deformation of deeper ridge geometry h ~ 13 µm

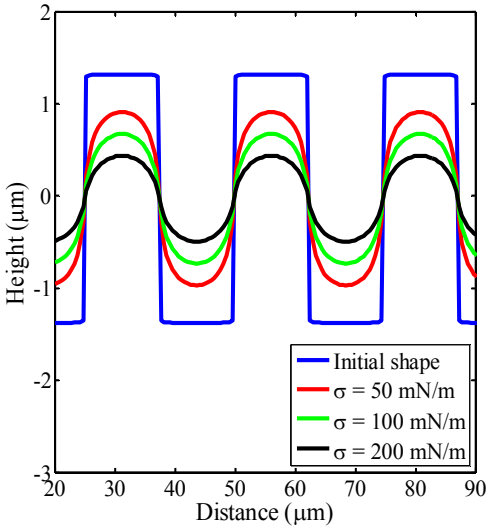

Figure 3: Prediction of final shape of the gel profile based on eq. [8] for a low height (h ~ 2.7 µm) periodic ridge geometry with Young's modulus E = 33 kPa and λ ~ 25 µm. Surface stress σ increases from 50 -200 mN/m.

Compliant materials are often structured by molding into a master made of much stiffer material and it is common for feature height to be about the same size as other dimensions such as width or spacing. For such cases, deformation can be significantly larger and its analysis requires numerical methods. Here we demonstrate that a finite element analysis of larger deformations can be used to model this more general situation of surface-stress-driven deformation.

A straightforward dimensional analysis shows that

$$\frac{h_d}{h} = f\left(\frac{\sigma}{\lambda E}, \frac{w}{\lambda}, \frac{h}{\lambda}\right) \quad [10]$$

where h_d is the deformed height for a ridge geometry with initial height h. In the case of shallow ridge, $\frac{h}{\lambda} \ll 1$, for the small-strain solution in eq. [9], the ratio

$$\frac{h_d}{h} = f\left(\frac{\sigma}{\lambda E}, \frac{h}{\lambda}\right)$$

is independent of h/λ. However, when h/λ is large, the Hertz approximation is no longer valid, hence eq. [9] is not applicable. For these high ridge geometries, we carried out FEM analysis with a two dimensional plane strain modelusing ABAQUS/Standard 6.8® to simulate the surface deformation. Since the length of the ridges is very long in comparison with its lateral dimensions, a plane strain model is used. The predicted deformed surface profile was fitted to that obtained by experiment using surface stress as a fitting parameter.

In all our simulations, the gel was modelled as an incompressible neo-Hookean material [20] with strain energy density function

$$W = \frac{\mu}{2}(I_1 - 3), \quad I_1 = \lambda_1^2 + \lambda_2^2 + \lambda_3^2 \quad [11]$$

where I_1 is the first invariant of the left Cauchy-Green deformation tensor, λ_i's are the principal stretch ratios and $\mu = E/3$ is the small strain shear modulus.

The surface stress, σ, is assumed to be a material constant independent of deformation and composition [3]. Surface tension was modelled by augmenting the finite element model by a set of user-defined 2-node linear surface elements, which discretize the exposed gel surface [21]. Since the deformed surface is a long cylinder, one of the principal curvatures is zero; let the other be denoted by κ. The tractions **T** on the deformed solid body are related to the rate of change of tangent **t** to the surface, i.e., the surface curvature, by the Young-Laplace equation

$$\mathbf{T} = \frac{\sigma d\mathbf{t}}{ds}, \quad [12]$$

where s is the arc length of the deformed cross-section curve. Hence the net nodal force applied on the body due to a small patch of surface spanning two surface elements is

$$\mathbf{F} = \int_1^2 \mathbf{T}\, ds = \sigma(\mathbf{t}_2 - \mathbf{t}_1) \quad [13]$$

where **t** is the tangent vector of the surface elements, 1 and 2 refer to the surface elements before and after the node [21].

Figure 4 shows the deformed shape of a typical demolded gel sample (E = 44 kPa, σ = 200 mN/m) predicted by FEM simulation.

Figure 5 shows the deformed surface profile calculated by FEM for a high ridge geometry (h =13 μm, λ =34.15 μm, w=11 μm, E = 44 kPa) in the experiment with increasing surface stress. As expected, larger value of surface stress causes more rounding at the edges and lower deformed height.

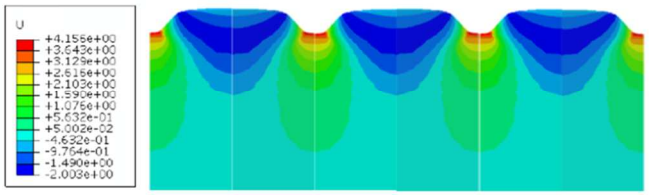

Figure 4: Deformed configuration of a typical demolded gel sample predicted by FEM simulation for E = 44 kPa, σ = 200 mN/m. Contours represents the vertical displacement U (μm).

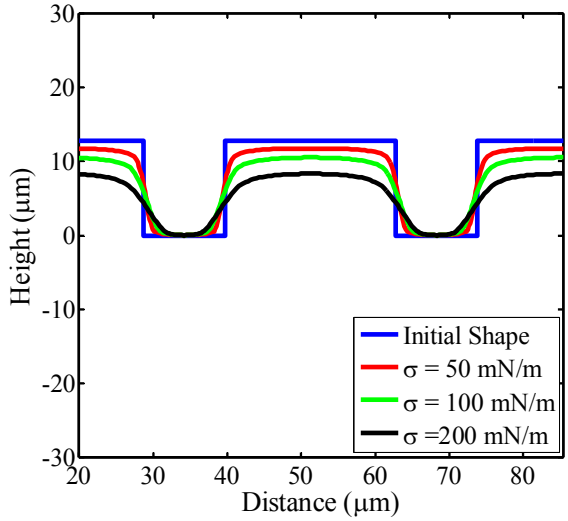

Figure 5: Simulation results for the shape deformation of the high periodic ridge geometry h = 13 μm) with a Young's modulus E = 44 kPa and λ =34.15 μm as a function of increasing surface stress.

Figure 6 shows the line scans (circle symbols) across the measured surface profile of a PDMS master and its gel replica (E = 35 kPa, λ ~ 35 μm) for the case of ridge height h ~ 13 μm. The least square fit results using FEM analysis are also presented alongside. The ratio of the deformed gel height h_d to the initial height h of the PDMS master (square symbols) is plotted in figure 6(b) for three different periodic spacing λ (symbols circles, triangles and inverted triangles represent, respectively, spacing of λ ~ 35, 50 and 65 μm, see Table 1) and five different moduli (E). Using least square fits based on the FEM model a surface stress value of 130.0±21.5 mN/m was estimated (lines in Figure 6(b)). The surface profile predicted by FEM simulation closely matches the experimental result as shown in Figure 6a. As previously stated, the precision of the fitted surface stress represents a 95% confidence interval [17]. The data showing the deformed gel heights h_d in comparison to their starting ridge height is given in SI . The values of surface stress obtained in this case are similar to those estimated for shallow ridge geometry.

FEM analysis for the case of h~ 2.7 μm (see SI) yielded a value of 105.0±17.6 mN/m for surface stress, in good agreement with that obtained using small strain theory, 100.0±9.4 mN/m. The difference in surface stress needed (130 mN/m) for the higher profile samples could be due to departure from the neo-Hookean model used – our purpose here is mainly to demonstrate that larger surface-stress deformations can be modelled numerically.

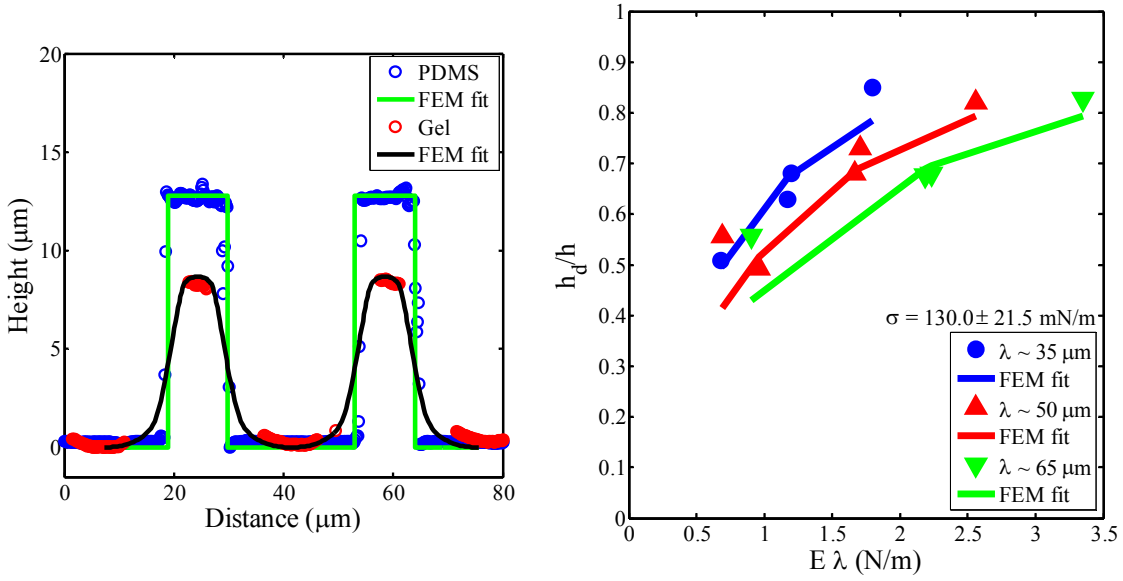

(a) **(b)**

Figure 6: (a) Line scans across measured surface profile of periodic ridge geometry for PDMS master and its gel replica (circle symbols) with E = 35 kPa, $\lambda \sim 35$ μm and initial height $h \sim 13$ μm. Predicted shape for the PDMS and gel profile (continuous lines) using FEM analysis. (b) Measured reduction in gel height (ratio of deformed to initial height (h_d/h) as a function of several elastic moduli (E) and periodic separations (λ, symbols circles, triangles and inverted triangles represent, respectively, spacing 35, 50 and 65 μm). Least square fit of FEM results to experimental data yields an estimate of the surface stress as 130.0±21.5 mN/m.

Discussion and Conclusions

We measured and characterized surface deformations in patterned organogels due to their surface stress. When a gel molded into a patterned (PDMS) master is subsequently separated from it, a new gel-air interface is created. This interface has a surface stress, in response to which the gel deforms, setting up internal stresses that balance the surface stress. We show that surface stress is able to drive significant deformation owing to the relatively low elastic moduli of the gels.

The characteristic strains encountered for samples with a shallow profile are on the order of $2\pi(h-h_d)/\lambda$,, which is small compared to unity, indicating that strains in the sample are generally small except at the corners, where strains are very large (if the corner is perfectly sharp, the strain is theoretically infinite). For shallow-profile samples, since h/λ <<1 and the average strain is small, we employed an analytical model based on periodic loading of a flat surface. The periodic surface is represented by Fourier series and the higher Fourier modes of the surface profile suffer greater deformation (eq. [3],[12]) [9,22]. The predicted gel profiles using small strain theory for shallow geometry as well as the FEM analysis in the high ridge geometry case match the experimentally measured profiles quite well (Figure 2b & 3a). We estimated surface stress σ =100.0±9.4 and 114.2±11.5 mN/m, respectively for h~ 2.7 and 1.7 μm (with average of the two estimates of surface stress σ= 107±7 mN/m).

For the case of high ridges (h~13 μm), the characteristic strains are moderately large, of the order of $2\pi(h-h_d)/h$ >100%. Using a FEM model in which the gel was assumed to be incompressible with neo-Hookean elasticity, we showed how such deformations can be modeled. We have assumed a single surface tension value for a given set of samples independent of their solid content and its surrogate, the elastic modulus. The quality of the resulting fits generally supports this hypothesis. Because the gel composition is dominated by the solvent, which constitutes roughly 90% of the solid gel, it would appear that surface stress should be determined primarily by surface tension of the water/glycerol mixture. However, the overall surface stress of 107±7 mN/m is significantly higher than that expected from the surface tension values of the glycerol/water mixture (for aqueous glycerol with ~60wt% glycerol, surface tension σ = 68.5 mN/m [23]). One possibility is that the ternary system (solid component and the two liquids that constitute the gel) forms significantly different structures. We hypothesize the formation of a new surface structure to explain the high overall stress. Water-glycerol mixtures with high concentration of glycerol (> 60 wt%) have been known to show enhancement of structured water[24]. Timasheff[25] found that a perturbation in the chemical potential of glycerol in the presence of the polypeptide protein gelatin results in the formation of new ternary phases consisting of water-gelatin-glycerol. Sanwlani et al. have shown, using Raman analysis, that for such a ternary system glycerol enhances structuring of water molecules (ice-like structure) causing gelatin molecules to compartmentalize to regions where glycerol-free water is available[24]. We point to the plausibility that a new structure of the water/glycerol/gel-

solid mixture could result in surface stress that differs from what one would expect from a rule of mixtures.

The confidence in the estimated surface stress values also depends on the accuracy and the precision of independently measured Young's moduli of the gels. Two methods, beam bending and load-displacement measurements with a flat punch were employed to determine the modulus. Possible inaccuracy in the independent measurement of the modulus limits the accuracy of the presented surface tension data.

The periodic ridge geometry is relatively easy to fabricate and so may serve as model for determination of surface stress of compliant solids. For cases where patterned surfaces are shallow ($h << \lambda$) the application of small strain elasticity theory successfully estimates the surface stress if the elastic properties of the gel are independently known. For the more general case, we have shown how finite element analysis can be used to analyse arbitrary deformation driven by surface tension.

Arrays of parallel channels are often fabricated in applications such as microfluidics using replica molding. Our work shows that when soft elastomer or gels are used in the fabrication, the shape of replica can be significantly different from the original mold. The analysis in the work presents a methodology to characterize the shape of these replicas.

Acknowledgements

This work was supported primarily by the U.S. Department of Energy, Office of Basic Energy Sciences, Division of Materials Science and Engineering under award DEFG02-07ER46463. DP was supported partially (1/3rd of his total time spent on this project) by INM-Leibniz Institute for New Materials and would like to thank Prof. E. Arzt for this support. AJ would like to acknowledge the suggestion of A. Ghatak (Indian Institute of Technology, Kanpur) for measurement of modulus by beam bending under its own weight.

Notes and references

[a] Department of Chemical Engineering, Lehigh University, Bethlehem PA 18015, USA.
[b] INM-Leibniz Institute for New Materials, Functional Surfaces Group, Campus D 2 2, 66123 Saarbruecken, Germany.
[c] Sibley School of Mechanical and Aerospace Engineering, [c1]Field of Theoretical and Applied Mechanics, Cornell University, Ithaca, New York 14853, USA.

1. R. Shuttleworth, *Proc. Phys. Soc. Sect. A*, 1950, **63**, 444.
2. R. C. Cammarata and K. Sieradzki, *Annu. Rev. Mater. Sci.*, 1994, **24**, 215–234.
3. C.-Y. Hui and a Jagota, *Langmuir*, 2013, **29**, 11310–6.
4. C. Y. Hui, A. Jagota, Y. Y. Lin, and E. J. Kramer, *Langmuir*, 2002, **18**, 1394–1407.
5. B. Roman and J. Bico, *J. Phys. Condens. Matter*, 2010, **22**, 493101.
6. S. Mora, T. Phou, J.-M. Fromental, L. M. Pismen, and Y. Pomeau, *Phys. Rev. Lett.*, 2010, **105**, 214301.
7. E. Jerison, Y. Xu, L. Wilen, and E. Dufresne, *Phys. Rev. Lett.*, 2011, **106**, 1–4.
8. A. Marchand, S. Das, J. H. Snoeijer, and B. Andreotti, *Phys. Rev. Lett.*, 2012, **108**, 094301.
9. A. Jagota, D. Paretkar, and A. Ghatak, *Phys. Rev. E*, 2012, **85**, 1–6.
10. J. . W. Gibbs, *On the equilibrium of heterogenous substances*, Longman, Green, 1928, London and New York, 1876, vol. I.
11. P.-G. DeGennes, F. Brochard-Wyart, and D. Quere, *Capillarity and Wetting Phenomena. Drops, Bubbles, Pearls, Waves.*, Springer Science+Business Media, Inc., New York, 2002.
12. R. W. Style, R. Boltyanskiy, Y. Che, J. S. Wettlaufer, L. a. Wilen, and E. R. Dufresne, *Phys. Rev. Lett.*, 2013, **110**, 066103.
13. N. Nadermann, C.-Y. Hui, and A. Jagota, *Proc. Natl. Acad. Sci. U. S. A.*, 2013, **110**, 10541–5.
14. A. K. Singh, Y. Bai, N. Nadermann, A. Jagota, and C.-Y. Hui, *Langmuir*, 2012, **28**, 4213–22.
15. T. Baumberger, C. Caroli, and D. Martina, *Nat. Mater.*, 2006, **5**, 552–5.
16. R. Long, C.-Y. Hui, S. Kim, and M. Sitti, *J. Appl. Phys.*, 2008, **104**, 044301–9.
17. H. J. C. Berendsen, *A student's Guide to Data and Error Analysis*, Cambridge University Press, 2011.
18. H. Hertz, *Miscellaneous Papers by H. Hertz*, Macmillian, London, 1896.
19. K. L. Johnson, *Contact Mechanics*, Cambridge University Press, 2003.
20. R. W. Ogden, *Non-linear Elastic Deformations*, Courier Dover, 1997.
21. X. Xu, A. Jagota, S. Peng, D. Luo, M. Wu, and C. Hui, *Langmuir*, 2013, **29**, 8665–74.
22. C. Y. Hui, A. Jagota, Y. Y. Lin, and E. J. Kramer, *Langmuir*, 2002, **18**, 1394–1407.
23. K. Takamura, H. Fischer, and N. R. Morrow, *J. Pet. Sci. Eng.*, 2012, **98-99**, 50–60.
24. S. Sanwlani, P. Kumar, and H. B. Bohidar, *J. Phys. Chem. B*, 2011, **115**, 7332–40.

25. S. N. Timasheff, *Proc. Natl. Acad. Sci. U. S. A.*, 2002, **99**, 9721–6.

Supplementary information

Determination of Young's modulus

a) Cylindrical Punch Indentation Experiment

The purpose of this brief note is to put down the relations needed to extract Young's modulus from a compliance measurement made by indenting a sample using a rigid cylindrical punch.

In the schematic figure S1, a circular cylindrical punch with radius a indents an elastic foundation that is very large in the plane of the contact, i.e., $L>>a$. However, its thickness, h, may or may not be large compared to a.

In the limit when $h>>a$, we have indentation by a rigid circular punch of an elastic half space. In this case [16,24],

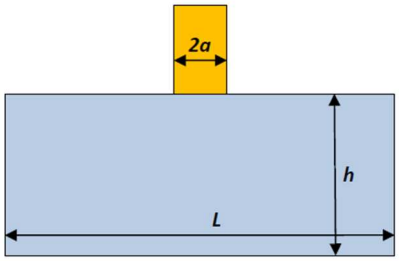

Figure S1: Schematic of flat cylindrical punch with diameter 2a used to indent a gel block of height h and diameter L

$$\lim_{h/a\to\infty}\left(\frac{d\delta}{dP}\right)=C_\infty=\frac{1}{2E^*a} \qquad [s1]$$

where δ is the displacement of the indenter, P is the measured load, C_∞ is the compliance in the limit $h>>a$ or $h/a\to\infty$, $E^*=E/(1-\nu^2)$ is the plane strain Young's modulus, and ν is Poisson's ratio. If the material is incompressible, then $\nu=1/2$, and equation s1 becomes

$$\lim_{h/a\to\infty}\left(\frac{d\delta}{dP}\right)=C_\infty=\frac{1}{2E^*a}=\frac{1-\nu^2}{2Ea}=\frac{3}{8Ea}=\frac{1}{8Ga} \qquad [s2]$$

where we have used the relation $G=E/(2(1+\nu))$. This is the same result as given in Long *et al.*[16] (equations 24 a, b) who have additionally shown that for finite h, the compliance C can be written in terms of C_∞ in the following way:

$$\frac{d\delta}{dP}=C=C_\infty\left(\frac{1}{1+\chi(\eta)}\right);\eta=\frac{a}{h} \qquad [s3]$$

$$\chi(\eta)=\frac{1.095\eta+1.3271\eta^2+0.1431\eta^4}{0.9717}$$

So, since C is the measured quantity, our expression for Young's modulus is

$$E^*=\frac{1}{2aC}\left(\frac{1}{1+\chi(\eta)}\right);\eta=\frac{a}{h} \qquad [s4]$$

$$\chi(\eta)=\frac{1.095\eta+1.3271\eta^2+0.1431\eta^4}{0.9717}$$

A typical load-displacement plot is shown in figure S2

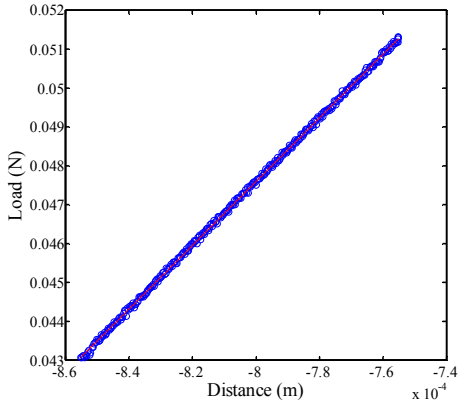

Figure S2: Load measured as a function of indentation depth (Distance) in a typical contact compliance test. The compliance C is the inverse of the slope.

b) Beam bending

The modulus was measured using the linear elastic moment-curvature relationship of beam theory

$$M=EIk \qquad [s5]$$

where M is the moment on the beam fixed at one end, I is the moment of inertia of the rectangular cross-section of the beam and k is the curvature of the bent element.

Equation (s5) can be re-written in terms of the distance s along the neutral axis of the beam

$$\frac{M(s)}{EI}=\frac{d\theta}{ds} \qquad [s6]$$

Integrating eq. s6

$$\int M(s)\,ds=EI\int d\theta \qquad [s7]$$

That is, the integral of the moment is linearly related to change in angle, and the slope is EI. The integral of the moment is plotted as a function of the angle and from the slope the modulus is obtained (figure S3).

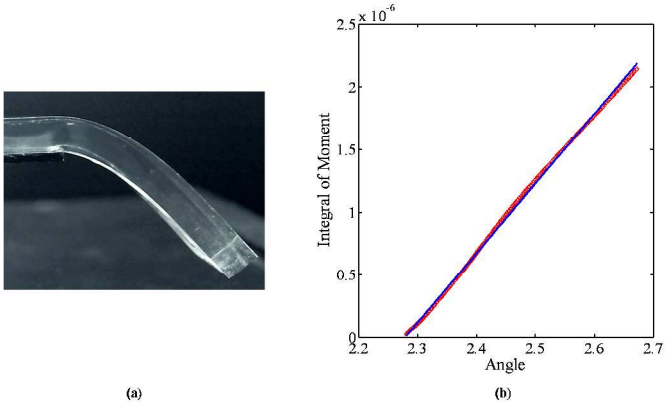

Figure S3: (a) Picture of a gel beam fixed at one end and freely hanging on the other (scale bar ~ 1cm). The profile of the beam is read using MATLAB code for determination of the curvature.

Gel filling of PDMS

We re-confirmed the assumption that the liquid gel wets the PDMS master completely. A section of the PDMS master was cut and laid flush on the bottom of the petri-dish such that the ridges were orientated perpendicular to it. After filling and gelation images were taken through the transparent base of the petri-dish. Figure S4 shows the optical micrographs of gel filled PDMS master.

Figure S4: Optical mircographs (scale bar 100 µm) of gel (E ~ 23 kPa) filled PDMS master prior to molding for periodic ridge geometry (a) h ~ 13 µm, λ ~ 35 µm and (a) h ~ 2.7 µm, λ ~ 25

High ridge geometry height reductions

In the experimental results part of the main text we noted the variation of the ratio of deformed to initial height for the high ridge geometry. Figure S5 shows the absolute heights of the PDMS and the deformed gel samples for the ridge geometry with h~ 13 µm. A lower deformed height (h_d) was measured for a gel with lower modulus (E).

FEM analysis for low height ridge geometry (h~ 2.7 µm)

To test the validity of the small strain theory, we applied also applied the FEM analysis to the case of shallow ridges for which small strain theory satisfactorily predicted the full deformed profile of the gel after demolding. Figure S6 shows that the least square fitting results of FEM analysis to experimental data yield a surface tension σ of 105.0±17.6 mN/m which quite similar to that obtained from the small strain theory (σ= 100.0±9.4 mN/m).

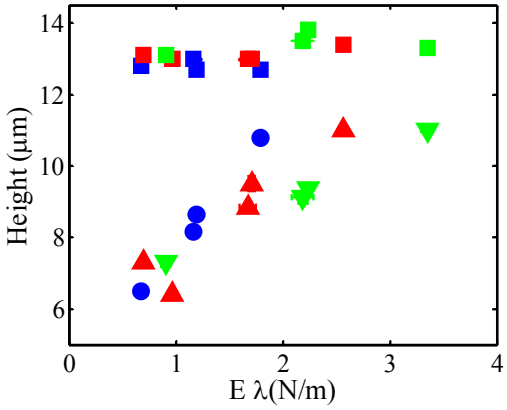

Figure S5: Measured initial height of ridge/channel in PDMS h ~ 13 µm (square symbols) and the corresponding gel height (h_d) for three different periodic spacing λ (symbols circles, triangles and inverted triangles represent, respectively, spacing of λ ~ 35, 50 and 65 µm, see Table 1 ($\lambda = s + w$) and five different moduli (E).

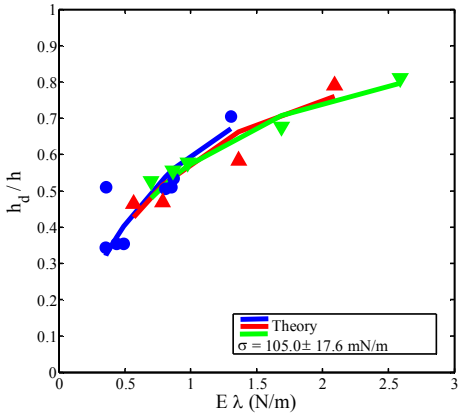

Figure S6: Measured reduction in gel height (ratio of final to initial height h/h_0) and FEM analysis based least square fits (continuous lines) for the height reduction as a function of varying elastic moduli E and three different periods λ

FEM analysis: Validity of neo-Hookean model

We applied an alternate model to the neo-Hookean to ascertain its validity. The linear elastic model was used to estimate the deformed heights (figure S6). We observe that for the surface tension of approx. 110 mN/m, which is close to estimated surface stress for low strain case, the two models deviate by less than 8% (figure S7). Thus there are limitations to the application of our technique to estimate surface stress using large deformations.

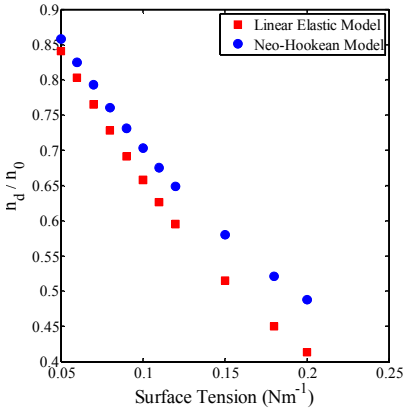

Figure S7: Comparison of deformed heights for a given surface tension for the neo-Hookean versus linear elastic material models.